

# Conformational biosensors reveal GPCR signalling from endosomes

Roshanak Irannejad<sup>1</sup>, Jin C. Tomshine<sup>1</sup>, Jon R. Tomshine<sup>1</sup>, Michael Chevalier<sup>2</sup>, Jacob P. Mahoney<sup>3</sup>, Jan Steyaert<sup>4,5</sup>, Søren G. F. Rasmussen<sup>6</sup>, Roger K. Sunahara<sup>3</sup>, Hana El-Samad<sup>2</sup>, Bo Huang<sup>2,7</sup> & Mark von Zastrow<sup>1,8</sup>

A long-held tenet of molecular pharmacology is that canonical signal transduction mediated by G-protein-coupled receptor (GPCR) coupling to heterotrimeric G proteins is confined to the plasma membrane. Evidence supporting this traditional view is based on analytical methods that provide limited or no subcellular resolution<sup>1</sup>. It has been subsequently proposed that signalling by internalized GPCRs is restricted to G-protein-independent mechanisms such as scaffolding by arrestins<sup>2,3</sup>, or GPCR activation elicits a discrete form of persistent G protein signalling<sup>4–9</sup>, or that internalized GPCRs can indeed contribute to the acute G-protein-mediated response<sup>10</sup>. Evidence supporting these various latter hypotheses is indirect or subject to alternative interpretation, and it remains unknown if endosome-localized GPCRs are even present in an active form. Here we describe the application of conformation-specific single-domain antibodies (nanobodies) to directly probe activation of the  $\beta_2$ -adrenoceptor, a prototypical GPCR<sup>11</sup>, and its cognate G protein,  $G_s$  (ref. 12), in living mammalian cells. We show that the adrenergic agonist isoprenaline promotes receptor and G protein activation in the plasma membrane as expected, but also in the early endosome membrane, and that internalized receptors contribute to the overall cellular cyclic AMP response within several minutes after agonist application. These findings provide direct support for the hypothesis that canonical GPCR signalling occurs from endosomes as well as the plasma membrane, and suggest a versatile strategy for probing dynamic conformational change *in vivo*.

Ligand binding to the extracellular surface of the  $\beta_2$ -adrenoceptor ( $\beta_2$ -AR) stabilizes an activating conformational change in the receptor that promotes guanine nucleotide dissociation from the cytoplasmic GTP-binding protein  $G_s$ ; this represents the critical biochemical event initiating classical GPCR signal transduction (Fig. 1a)<sup>13</sup>. Activated  $\beta_2$ -ARs are substrates for phosphorylation and binding of  $\beta$ -arrestins, events which inhibit interaction with G proteins and promote endocytosis of receptors via clathrin-coated pits (CCPs)<sup>14,15</sup>. Acute  $\beta_2$ -AR  $G_s$  signalling is thus traditionally thought to be restricted to the plasma membrane<sup>14,16,17</sup>. However, to our knowledge, this assumption has not been directly tested. To do so, we generated a biosensor of activated  $\beta_2$ -AR based on a conformation-specific single-domain camelid antibody (Nb80) used in recent structural studies<sup>18,19</sup>. We reasoned that this nanobody, which selectively binds the agonist-occupied  $\beta_2$ -AR and is able to stabilize an activated receptor conformation when present *in vitro* at high concentration, might act as a sensor of receptor activation when expressed at relatively low concentration in intact cells (Fig. 1b). This proved to be the case; in cells maintained in the absence of agonist, Nb80 fused to enhanced green fluorescent protein (Nb80-GFP) localized to the cytoplasm and not with  $\beta_2$ -ARs present in the plasma membrane (Fig. 1c, 0 min, top; Pearson's coefficient = 0.135). Line scan analysis verified the cytoplasmic distribution of Nb80-GFP before  $\beta_2$ -AR activation (Fig. 1d, top) as expected because the

cytoplasmic concentration of Nb80-GFP achieved in our experiments (approximately 20 nM) was considerably lower than the equilibrium dissociation constant estimated *in vitro* for Nb80 binding to purified  $\beta_2$ -ARs in the absence of agonist ( $0.76 \pm 0.14 \mu\text{M}$ ; Supplementary Fig. 1a–d). After application of the adrenergic agonist isoprenaline (10  $\mu\text{M}$ ), Nb80-GFP was rapidly recruited to the plasma membrane and co-localized there with  $\beta_2$ -ARs (Fig. 1c, middle; Pearson's coefficient = 0.625). Line scan analysis verified robust Nb80-GFP recruitment to the plasma membrane and concomitant depletion from the cytoplasm (Fig. 1d, middle), consistent with the much higher affinity of Nb80 for isoprenaline-activated  $\beta_2$ -ARs ( $2.9 \pm 0.5 \text{ nM}$ ; Supplementary Fig. 1d). Agonist-induced membrane recruitment of Nb80-GFP was specific because the D1 dopamine receptor (DRD1), which is also  $G_s$ -coupled but does not bind Nb80 *in vitro* (data not shown), failed to recruit Nb80-GFP to the plasma membrane in response to dopamine (10  $\mu\text{M}$ ) application (Supplementary Fig. 2). Furthermore,  $\beta_2$ -AR-cyan fluorescent protein (CFP) and Nb80-yellow fluorescent protein (YFP) generated a pronounced fluorescence (Förster) resonance energy transfer (FRET) signal after isoprenaline application whereas DRD1-CFP did not (Supplementary Fig. 3a, b).

$\beta_2$ -AR internalization began 1 to 2 min after Nb80-GFP recruitment to the plasma membrane, indicated by the emergence of surface-labelled  $\beta_2$ -AR in peripheral cytoplasmic vesicles. Nb80-GFP did not co-localize with  $\beta_2$ -AR-containing endocytic vesicles upon first appearance (Fig. 1c, middle, arrow in merged image points to an example) but was recruited at later time points (Fig. 1c, bottom, Pearson's coefficient = 0.702; examples are indicated by arrowheads). Endosome recruitment of Nb80-GFP was evident by line scan analysis (Fig. 1d, bottom; line scans are from the representative individual examples with further quantification in legend) and localized to EEA1-marked early endosomes (Pearson's coefficient = 0.846; Supplementary Fig. 4) through which  $\beta_2$ -ARs iteratively cycle in the presence of agonist<sup>20</sup>.  $\beta_2$ -AR-containing endosomes were initially devoid of Nb80-GFP and later acquired Nb80-GFP during their movement (Supplementary Videos 1 and 2). Interaction at endosomes was verified by  $\beta_2$ -AR-CFP and Nb80-YFP normalized FRET (nFRET) (Supplementary Fig. 3c). These results suggest that  $\beta_2$ -AR activation initiates a precisely choreographed series of events: Nb80-GFP is first recruited from the cytoplasm to the plasma membrane, then  $\beta_2$ -ARs internalize devoid of Nb80-GFP, followed by a second phase of Nb80-GFP recruitment to the internalized  $\beta_2$ -ARs.

Nb80-GFP recruitment to endosomes required  $\beta_2$ -ARs because a phosphorylation-deficient mutant version of the  $\beta_2$ -AR ( $\beta_2$ -AR-3S, with three serine mutations) that couples to  $G_s$  but is impaired in agonist-induced endocytosis<sup>21</sup> recruited Nb80-GFP to the plasma membrane but produced much less recruitment to endosomes (Fig. 1e, top). Nb80-GFP co-localized with  $\beta_2$ -AR-3S after agonist-induced activation (Pearson's coefficient = 0.674) but this was largely restricted to the

<sup>1</sup>Department of Psychiatry, University of California, San Francisco, California 94158, USA. <sup>2</sup>Department of Biochemistry & Biophysics, University of California, San Francisco, California 94158, USA.

<sup>3</sup>Department of Pharmacology, University of Michigan Medical School, Ann Arbor, Michigan 48109, USA. <sup>4</sup>Department of Molecular and Cellular Interactions, Vrije Universiteit Brussel, B-1050 Brussels, Belgium. <sup>5</sup>Structural Biology Research Centre, VIB, B-1050 Brussels, Belgium. <sup>6</sup>Department of Neuroscience and Pharmacology, The Panum Institute, University of Copenhagen, 2200 Copenhagen N, Denmark. <sup>7</sup>Department of Pharmaceutical Chemistry, University of California, San Francisco, California 94158, USA. <sup>8</sup>Department of Cellular & Molecular Pharmacology, University of California, San Francisco, California 94158, USA.

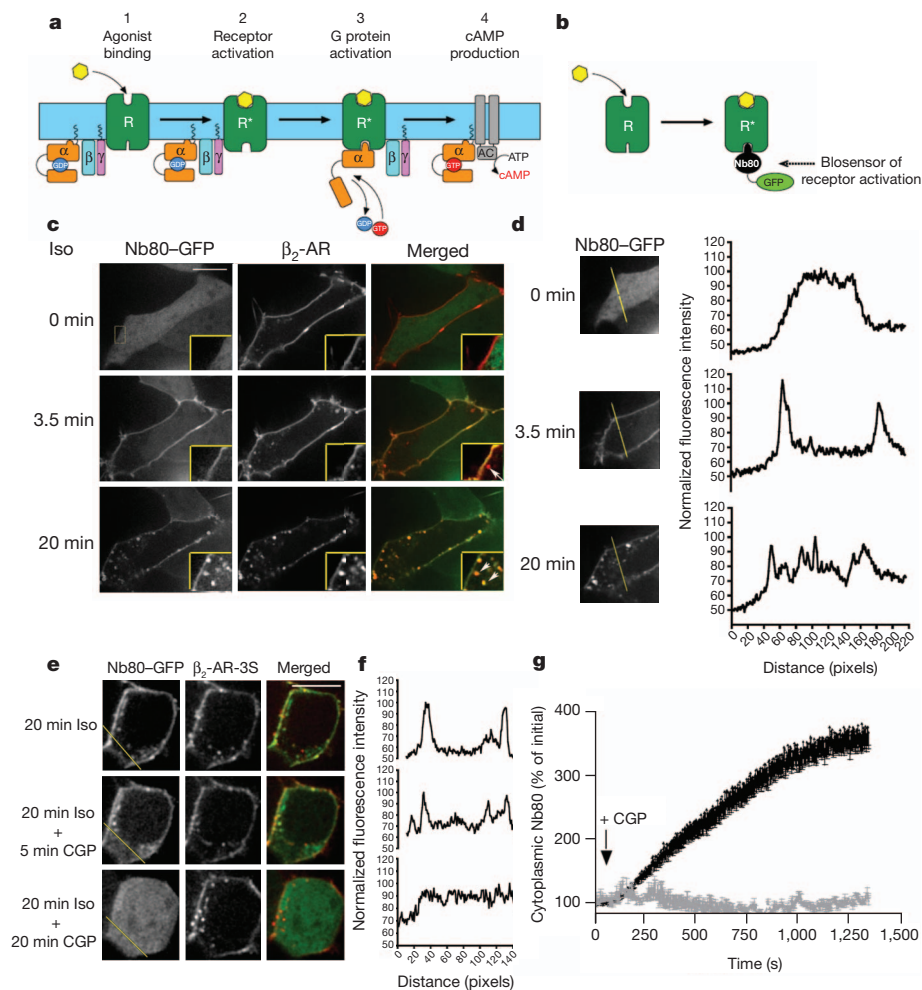


**Figure 1 | Nb80-GFP detects activated  $\beta_2$ -ARs in the plasma membrane and endosomes.** **a**, The main events in  $\beta_2$ -AR cAMP signalling include agonist binding (step 1), conformational activation of the receptor (step 2) that is coupled to conformational activation of  $G_s$  (step 3) that produces guanine nucleotide exchange on  $G_s$  and subsequent activation of adenylyl cyclase (AC) (step 4). **b**, Scheme for detecting conformational activation of  $\beta_2$ -AR with Nb80-GFP. **c**, Representative Nb80-GFP (green) and  $\beta_2$ -AR (red) localization at the indicated time (left) after 10  $\mu$ M isoprenaline addition (>30 Nb80-GFP positive endosomes per cell observed at 20 min;  $n = 29$  cells, 10 experiments). **d**, Representative individual Nb80-GFP line scans (shown at the same magnification as panel **c**). **e**, Representative Nb80-GFP (green) and  $\beta_2$ -AR-3S (red) localization after 20 min of isoprenaline treatment (top) followed by reversal with 50  $\mu$ M CGP-12177 for the indicated times (6.4 Nb80-GFP positive endosomes per cell;  $n = 40$  cells, 3 experiments). **f**, Representative individual Nb80-GFP line scans. **g**, Recovery of cytoplasmic Nb80-GFP fluorescence (black) or bleaching control of the plasma membrane  $\beta_2$ -AR-3S (grey) (mean  $\pm$  s.e.m.,  $n = 5$  experiments). Scale bars, 10  $\mu$ m.

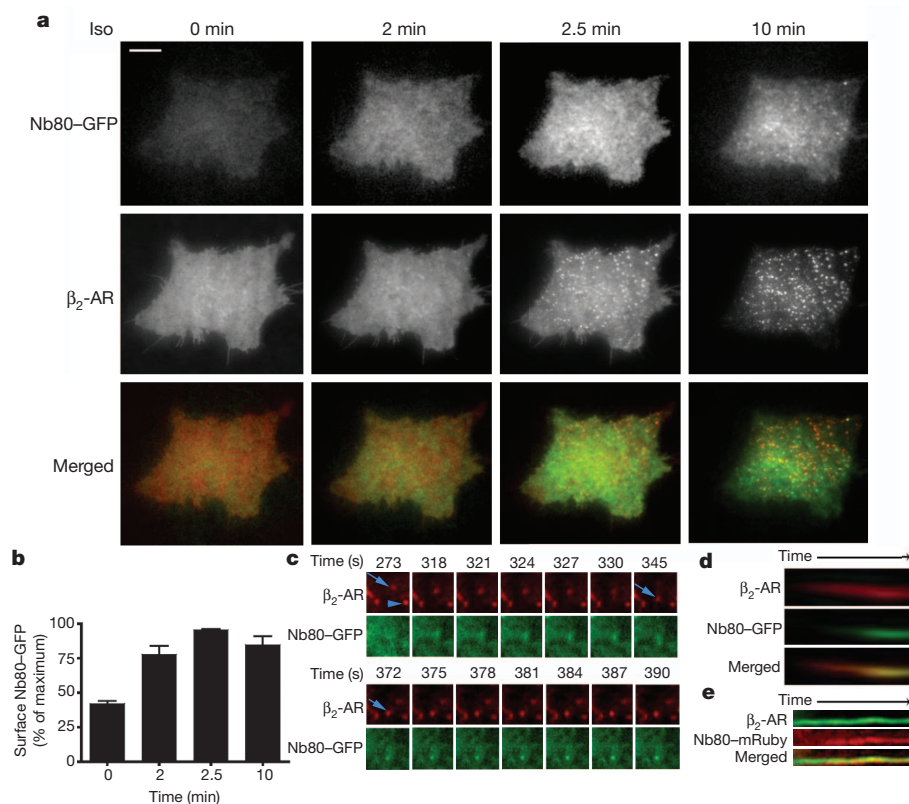


**Figure 2 | Nb80-GFP accumulates on  $\beta_2$ -AR-containing endosomes after their formation.** **a**,  $\beta_2$ -AR (red) and Nb80-GFP (green) at the indicated times after isoprenaline addition. Scale bar, 10  $\mu$ m. **b**, Average Nb80-GFP fluorescence measured in the TIRF illumination field at the indicated times (mean  $\pm$  s.e.m.,  $n = 7$  cells). **c**, TIRF image series showing  $\beta_2$ -AR (red) and Nb80-GFP (green) in sequential frames. **d**, Kymograph of an individual  $\beta_2$ -AR-containing endosome (red, Alexa555) showing Nb80-GFP (green) acquisition over 4 min. **e**, Kymograph of  $\beta_2$ -AR (green, Alexa488) and Nb80-mRuby (red) over 6 min.



plasma membrane (line scan analysis in Fig. 1f is representative; further quantification in the figure legend). Nb80–GFP membrane recruitment was also reversible because the biosensor returned to a cytoplasmic distribution after addition of the competitive antagonist CGP-12177 (Fig. 1e, f, middle and bottom rows; Pearson's coefficient = 0.106), verified by recovery of Nb80–GFP fluorescence intensity in the cytoplasm (Fig. 1g, see also Supplementary Video 3). Thus, Nb80–GFP detected activated  $\beta_2$ -ARs both in the plasma membrane and endosomes after acute agonist application.

Discrete Nb80–GFP recruitment phases were clearly resolved by total internal reflection fluorescence (TIRF) microscopy that selectively detects events occurring in the plasma membrane and extending approximately 100 nm into the peripheral cytoplasm<sup>22</sup>. First, within 2 min after agonist application, Nb80–GFP was progressively recruited to the plasma membrane in a diffuse distribution (Fig. 2a, compare first and second columns from left; quantification in Fig. 2b). Nb80–GFP did not co-localize with  $\beta_2$ -ARs when they clustered in relatively static punctae characteristic of receptor-containing CCPs<sup>23</sup> (Fig. 2a, third column). Second, over a period of several additional minutes, Nb80–GFP was recruited to a discrete population of highly mobile punctae (Fig. 2a, fourth column) representing peripheral  $\beta_2$ -AR-containing endocytic vesicles<sup>23</sup>.

Sequential TIRF imaging emphasized the distinction between relatively static  $\beta_2$ -AR puncta not co-localizing with Nb80–GFP (Fig. 2c, arrowhead indicates an example) and mobile endosomes that did (Fig. 2c, arrow indicates a representative example; many are visible in Supplementary Video 4). Later recruitment of Nb80–GFP occurred rather suddenly, typically within approximately 5 s (Supplementary Video 5), as also evident in kymographs of individual endosome trajectories (Fig. 2d). Ruling out potential artefacts of wavelength-dependent differences in TIRF microscopy illumination depth, later recruitment of the biosensor to endosomes was similarly observed when the excitation wavelengths used to detect receptor and biosensor were reversed (Fig. 2e).

Nb80–GFP did not detectably concentrate in CCPs labelled with either of two independent markers, the adaptor protein  $\beta$ -arrestin-2 (Fig. 3a and Supplementary Video 6) or the coat protein component clathrin light chain (Fig. 3b and Supplementary Video 7). Representative examples are shown and this was verified across multiple cells and experiments (Pearson's coefficient = 0.365 and 0.319, respectively, with numbers of replicates specified in the legend). In contrast, and as expected based on previous work, extensive co-localization of  $\beta_2$ -AR with  $\beta$ -arrestin was observed under the same conditions (Pearson's coefficient = 0.677). Separation of Nb80–GFP localization from that of either  $\beta$ -arrestin or clathrin was clear in line scans (bottom panels of Fig. 3a, b were derived from the images shown and are representative, further quantification is in the legend).

A simple interpretation is that Nb80–GFP associates with activated  $\beta_2$ -ARs in the plasma membrane but then dissociates before receptors cluster in CCPs and internalize. This was surprising because  $\beta_2$ -AR clustering in CCPs occurs much more rapidly<sup>23</sup> than the overall reversal rate of Nb80–GFP recruitment observed after agonist washout in intact cells (Fig. 1g), or the kinetics of Nb80 dissociation from purified  $\beta_2$ -ARs *in vitro* (Supplementary Fig. 1b, e). One possibility is that Nb80–GFP dissociation is accelerated during the clustering process, by mechanisms such as receptor phosphorylation or steric exclusion mediated by  $\beta$ -arrestins or other CCP-associated components. An alternative possibility is that the fraction of  $\beta_2$ -ARs that have bound Nb80–GFP in the plasma membrane by the time of the clustering reaction are unable to enter CCPs, and only those  $\beta_2$ -ARs not initially bound to Nb80–GFP in the plasma membrane are able to cluster in CCPs and subsequently internalize. In either case, the data clearly indicate that Nb80–GFP associates with  $\beta_2$ -ARs after endocytosis, and after uncoating of the endocytic vesicle has occurred (Fig. 3c). Accordingly, Nb80–GFP recruitment to  $\beta_2$ -AR-containing endosomes cannot represent an artefact of persistent nanobody binding from the plasma membrane; instead, this observation reveals that  $\beta_2$ -ARs present in early endosomes are in an activated conformation.

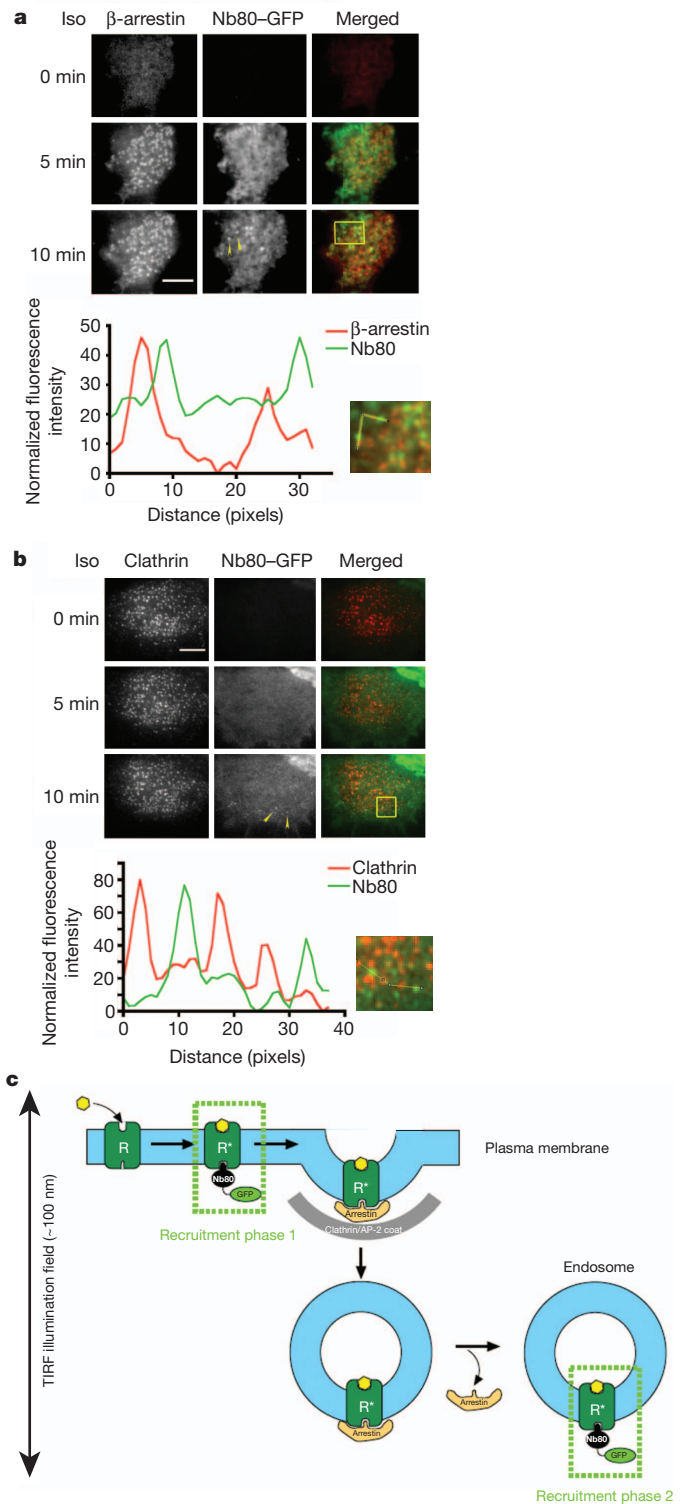


**Figure 3 | Nb80–GFP does not accumulate in clathrin-coated pits or vesicles.** **a**, Representative TIRF microscopy frames showing Nb80–GFP (green) and  $\beta$ -arrestin-2-mCherry (red) before and after agonist addition. Fluorescence intensity profiles are shown below for the indicated region and path; representative of  $n = 39$  cells, 5 experiments and 4,849 punctae. **b**, Equivalent analysis comparing Nb80–GFP (green) to clathrin light chain-dsRed (red); representative of  $n = 26$  cells, 3 experiments and 3,965 punctae. Arrowheads indicate examples of Nb80–GFP labelled endosomes. Scale bars, 5  $\mu$ m. **c**, Model for two phases of Nb80–GFP recruitment by the activated  $\beta_2$ -AR, first at the plasma membrane and then at endosomes.

Because endosomes contain activated  $\beta_2$ -ARs, we next asked if receptors engage their cognate G protein from this compartment. Heterotrimeric G proteins and adenylyl cyclase can be observed in endosomes as well as at the plasma membrane, supporting the concept of endosome-based G protein signalling<sup>4,6,10,24</sup>. To directly investigate the subcellular location of G protein activation, we developed a distinct biosensor based on another nanobody, Nb37, which specifically recognizes the guanine-nucleotide-free form of  $G\alpha_s$  representing the catalytic intermediate of G protein activation (Fig. 4a)<sup>25</sup>. We hoped that, because Nb37 binds a surface of the alpha-helical domain that is accessible only in the nucleotide-free form, we would be able to detect production of this critical but fleeting activation intermediate in living cells. This was indeed the case because Nb37-GFP localized in the cytoplasm of untreated cells and was rapidly recruited from the cytoplasm to the plasma membrane in response to isoprenaline application (Fig. 4b, yellow arrowhead, Pearson coefficient = 0.627). Membrane recruitment of Nb37-GFP was agonist-dependent even in cells overexpressing  $G\alpha_s$  and, notably, the cytoplasmic concentration of Nb37-GFP achieved in our experiments (also approximately 20 nM) was substantially lower than that producing detectable inhibition of G protein activation *in vitro* (Supplementary Fig. 5). Together, these observations suggest that Nb37-GFP indeed functions as a specific biosensor of  $G_s$  activation under the experimental conditions used.

Nb37-GFP was recruited not only to the plasma membrane (Fig. 4b, yellow arrowhead) but also to  $\beta_2$ -AR-containing endosomes. Notably, endosome recruitment of Nb37-GFP occurred after the appearance of  $\beta_2$ -ARs in the endosome. Such later recruitment was evident in dual label confocal image series (Fig. 4b shows an example: white arrowhead indicates recently internalized  $\beta_2$ -AR, white arrows indicate Nb37-GFP recruitment, Pearson coefficient = 0.710; see also Supplementary Video

8). Nb37-GFP recruitment was specifically dependent on receptor activation because a mutant  $\beta_2$ -AR that is defective in G-protein coupling ( $\beta_2$ -AR-Cys 341 Gly)<sup>26</sup> did not produce detectable recruitment (Supplementary Fig. 6), whereas the distinct  $G_s$ -coupled DRD1 recruited Nb37-GFP to both the plasma membrane and endosomes (data not shown). Nb37-GFP localized uniformly on  $\beta_2$ -AR-containing endosomes in cells overexpressing  $G\alpha_s$  (Fig. 4b and Supplementary Video 8) but was recruited non-uniformly in cells expressing endogenous levels (Fig. 4c, arrowhead indicates an example). Moreover, Nb37-GFP recruitment to endosomes had a scintillating appearance, fluctuating rapidly when viewed in live image series (Supplementary Video 9), suggesting that G protein activation detected by Nb37-GFP occurs dynamically from limited regions of the endosome membrane.

We then asked if active  $\beta_2$ -AR  $G_s$  coupling from endosomes contributes to the cellular response, focusing on cAMP as a classical second messenger carrying the downstream signal, using a previously described real-time assay of cAMP accumulation in living cells and normalizing to the signal produced by receptor-independent activation of adenylyl cyclase with forskolin (5  $\mu$ M)<sup>27</sup>. Isoprenaline produced a rapid increase in cytoplasmic cAMP accumulation, reaching a maximum within approximately 10 min (Fig. 4d, blue line). Dyngo-4a, a dynamin inhibitor that blocks  $\beta_2$ -AR endocytosis by inhibiting CCP function<sup>28,29</sup>, did not detectably affect the earliest portion of the forskolin-normalized cAMP accumulation curve but significantly reduced its later rise (Fig. 4d, green line, grey dots indicate *P* values), consistent with the two phases of endosome-localized activation detected by the nanobody-derived biosensors. A similar inhibition was observed in cells expressing a mutant  $\beta_2$ -AR with a carboxy-terminal alanine residue added that prevents efficient recycling

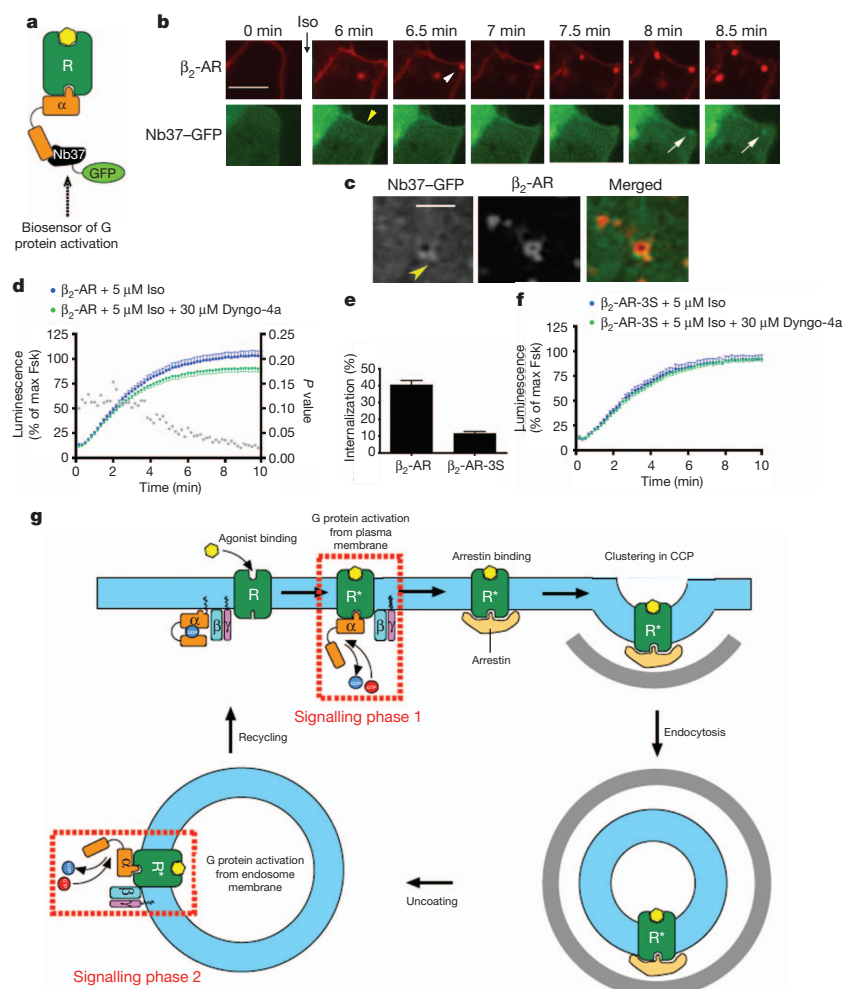


**Figure 4 | Internalized  $\beta_2$ -ARs contribute to the acute cAMP response.** **a**, Scheme for detecting conformational activation of  $G_s$  with Nb37-GFP. **b**, Confocal image frames showing Nb37-GFP (green) and  $\beta_2$ -AR (red) at the indicated time points after isoprenaline addition (representative of  $n = 14$  cells; estimated Nb37-GFP recruitment delay ranged from 0.7 to 2.65 min). Scale bar, 5  $\mu$ m. Yellow arrowhead indicates Nb37-GFP recruitment to the plasma membrane. White arrowhead indicates an endosome containing recently internalized  $\beta_2$ -AR and not associated with Nb37-GFP, white arrows indicate Nb37-GFP recruitment. **c**, Representative confocal frames showing a discrete endosomal structure labelled with Nb37-GFP (green) and  $\beta_2$ -AR (red) at higher magnification. Scale bar, 2  $\mu$ m. Arrowhead indicates non-uniform localization of Nb37-GFP to the endosome. **d**, Forskolin-normalized  $\beta_2$ -AR-mediated cAMP response in the absence or presence of 30  $\mu$ M Dyngo-4a (mean  $\pm$  s.e.m.,  $n = 10$  experiments, *P* values in grey). **e**, Isoprenaline (20 min)-induced  $\beta_2$ -AR and  $\beta_2$ -AR-3S internalization measured by flow cytometry ( $n = 4$  experiments). **f**, Forskolin-normalized  $\beta_2$ -AR-3S-mediated cAMP response in the absence or presence of 30  $\mu$ M Dyngo-4a ( $n = 8$  experiments;  $P = 0.1192$ ). **g**, Model for two phases of  $\beta_2$ -AR  $G_s$  activation, first at the plasma membrane and then at endosomes, separated by the endocytic event.



( $\beta_2$ -AR-Ala)<sup>30</sup> (Supplementary Fig. 7), suggesting that the Dyngo-sensitive component of the cAMP response did not represent a secondary consequence of resensitization by receptor recycling<sup>17</sup>. Dyngo-4a did not produce the same effect on cAMP accumulation elicited by the internalization-defective  $\beta_2$ -AR-3S mutant receptor<sup>21</sup> (Fig. 4e, f), further supporting the conclusion that the second signalling phase indeed requires receptor localization in endosomes.

The present findings revise a long-held tenet of molecular pharmacology, that acute signal transduction mediated by the canonical  $\beta_2$ -AR  $G_s$  signal transduction mechanism is plasma membrane delimited. The results provide direct evidence supporting the hypothesis that  $\beta_2$ -AR endocytosis contributes to a second phase of the acute cellular cAMP response, which represents a significant component of the overall biochemical signal developed within several minutes after the initial agonist application. Thus, although it remains clear that  $\beta_2$ -ARs can elicit  $G_s$ -mediated signal transduction from the plasma membrane, the present data reveal a discrete component of the acute signalling response that is initiated from endosomes (Fig. 4g). It remains unknown if  $\beta_2$ -ARs are continuously bound by agonist in endosomes, as depicted in the figure for simplicity, but conformational activation of  $G_s$  in endosomes is both receptor- and agonist-dependent. Unambiguous detection of endosome-based activation of acute G-protein-linked signalling is presently limited to the  $\beta_2$ -AR  $G_s$  system for which the critical nanobodies are available. However, endosome-based contribution to the acute signalling response is probably widespread in the GPCR superfamily because the  $\beta_2$ -AR belongs to the largest group (family A) of GPCRs and is often considered a prototype. We also suggest, more generally, that nanobody-based biosensors represent a versatile strategy for probing other types of dynamic conformational change with high spatiotemporal resolution in living cells.

## METHODS SUMMARY

Experiments were carried out using human embryonic kidney HEK293 cells (ATCC) expressing the indicated receptor constructs and nanobodies fused to enhanced GFP. Optical imaging was carried out at 37 °C in DMEM not containing phenol red and supplemented with 30 mM HEPES. Live cell cAMP accumulation was assessed at 37 °C using pGloSensor-20F (Promega). Flow cytometry was carried out using Alexa647 (Invitrogen)-conjugated M1 anti-Flag monoclonal antibody (Sigma) and a FACSCalibur instrument (Becton Dickinson).

**Full Methods** and any associated references are available in the online version of the paper.

Received 13 August 2012; accepted 8 February 2013.

Published online 20 March 2013.

- Lohse, M. J., Nuber, S. & Hoffmann, C. Fluorescence/bioluminescence resonance energy transfer techniques to study G-protein-coupled receptor activation and signaling. *Pharmacol. Rev.* **64**, 299–336 (2012).
- Shenoy, S. K. & Lefkowitz, R. J. Seven-transmembrane receptor signaling through  $\beta$ -arrestin. *Sci. STKE* **2005**, cm10 (2005).
- Murphy, J. E., Padilla, B. E., Hasdemir, B., Cottrell, G. S. & Bunnett, N. W. Endosomes: a legitimate platform for the signaling train. *Proc. Natl Acad. Sci. USA* **106**, 17615–17622 (2009).
- Ferrandon, S. et al. Sustained cyclic AMP production by parathyroid hormone receptor endocytosis. *Nature Chem. Biol.* **5**, 734–742 (2009).
- Feinstein, T. N. et al. Retromer terminates the generation of cAMP by internalized PTH receptors. *Nature Chem. Biol.* **7**, 278–284 (2011).
- Calebiro, D. et al. Persistent cAMP-signals triggered by internalized G-protein-coupled receptors. *PLoS Biol.* **7**, e1000172 (2009).
- Werthmann, R. C., Volpe, S., Lohse, M. J. & Calebiro, D. Persistent cAMP signaling by internalized TSH receptors occurs in thyroid but not in HEK293 cells. *FASEB J.* **26**, 2043–2048 (2012).
- Müllershausen, F. et al. Persistent signaling induced by FTY720-phosphate is mediated by internalized S1P1 receptors. *Nature Chem. Biol.* **5**, 428–434 (2009).
- Calebiro, D., Nikolaev, V. O. & Lohse, M. J. Imaging of persistent cAMP signaling by internalized G protein-coupled receptors. *J. Mol. Endocrinol.* **45**, 1–8 (2010).
- Kotowski, S. J., Hopf, F. W., Seif, T., Bonci, A. & von Zastrow, M. Endocytosis promotes rapid dopaminergic signaling. *Neuron* **71**, 278–290 (2011).
- Lefkowitz, R. J. Seven transmembrane receptors: something old, something new. *Acta Physiol. (Oxf.)* **190**, 9–19 (2007).

- Gilman, A. G. Transmembrane signaling, G proteins, and adenylyl cyclase. *Harvey Lect.* **85**, 153–172 (1989).
- Rasmussen, S. G. et al. Crystal structure of the  $\beta_2$  adrenergic receptor-Gs protein complex. *Nature* **477**, 549–555 (2011).
- Moore, C. A., Milano, S. K. & Benovic, J. L. Regulation of receptor trafficking by GRKs and arrestins. *Annu. Rev. Physiol.* **69**, 451–482 (2007).
- Sorkin, A. & von Zastrow, M. Endocytosis and signalling: intertwining molecular networks. *Nature Rev. Mol. Cell Biol.* **10**, 609–622 (2009).
- Luttrell, L. M. & Lefkowitz, R. J. The role of  $\beta$ -arrestins in the termination and transduction of G-protein-coupled receptor signals. *J. Cell Sci.* **115**, 455–465 (2002).
- Gainetdinov, R. R., Premont, R. T., Bohn, L. M., Lefkowitz, R. J. & Caron, M. G. Desensitization of G protein-coupled receptors and neuronal functions. *Annu. Rev. Neurosci.* **27**, 107–144 (2004).
- Rasmussen, S. G. et al. Structure of a nanobody-stabilized active state of the  $\beta_2$  adrenoceptor. *Nature* **469**, 175–180 (2011).
- Steyaert, J. & Kobilka, B. K. Nanobody stabilization of G protein-coupled receptor conformational states. *Curr. Opin. Struct. Biol.* **21**, 567–572 (2011).
- Lauffer, B. E. et al. SNX27 mediates PDZ-directed sorting from endosomes to the plasma membrane. *J. Cell Biol.* **190**, 565–574 (2010).
- Hausdorff, W. P. et al. A small region of the  $\beta$ -adrenergic receptor is selectively involved in its rapid regulation. *Proc. Natl Acad. Sci. USA* **88**, 2979–2983 (1991).
- Steyer, J. A. & Almers, W. A real-time view of life within 100 nm of the plasma membrane. *Nature Rev. Mol. Cell Biol.* **2**, 268–275 (2001).
- Puthenveedu, M. A. & von Zastrow, M. Cargo regulates clathrin-coated pit dynamics. *Cell* **127**, 113–124 (2006).
- Slessareva, J. E., Routt, S. M., Temple, B., Bankaitis, V. A. & Dohman, H. G. Activation of the phosphatidylinositol 3-kinase Vps34 by a G protein  $\alpha$  subunit at the endosome. *Cell* **126**, 191–203 (2006).
- Westfield, G. H. et al. Structural flexibility of the  $G_{s\alpha}$  helical domain in the  $\beta_2$ -adrenoceptor  $G_s$  complex. *Proc. Natl Acad. Sci. USA* **108**, 16086–16091 (2011).
- Campbell, P. T. et al. Mutations of the human  $\beta_2$ -adrenergic receptor that impair coupling to  $G_s$  interfere with receptor down-regulation but not sequestration. *Mol. Pharmacol.* **39**, 192–198 (1991).
- Violin, J. D. et al.  $\beta_2$ -adrenergic receptor signaling and desensitization elucidated by quantitative modeling of real time cAMP dynamics. *J. Biol. Chem.* **283**, 2949–2961 (2008).
- Harper, C. B. et al. Dynamin inhibition blocks botulinum neurotoxin type A endocytosis in neurons and delays botulism. *J. Biol. Chem.* **286**, 35966–35976 (2011).
- Howes, M. T. et al. Clathrin-independent carriers form a high capacity endocytic sorting system at the leading edge of migrating cells. *J. Cell Biol.* **190**, 675–691 (2010).
- Cao, T. T., Deacon, H. W., Reczek, D., Bretscher, A. & von Zastrow, M. A kinase-regulated PDZ-domain interaction controls endocytic sorting of the  $\beta_2$ -adrenergic receptor. *Nature* **401**, 286–290 (1999).

**Supplementary Information** is available in the online version of the paper.

**Acknowledgements** We thank B. Kobilka, P. Robinson, A. Kruse, E. Pardon, P. Temkin, M. Puthenveedu, A. Henry, A. Marley and K. Thorn for assistance, advice and discussion. These studies were supported by the National Institute on Drug Abuse of the US National Institutes of Health (DA010711 and DA012864 to M.v.Z. and F32 DA029993 to J.C.T.). R.I. is supported by the American Heart Association. R.K.S. and J.P.M. are supported by the National Institute of General Medical Sciences (GM083118 to R.K.S. and T32 GM007767 to J.P.M.). S.G.F.R. is supported by the Lundbeck Foundation. J.S. is supported by FWO-Vlaanderen grants (FWO551 and FWO646) and Innoviris-Brussels (BRGE02132). B.H. is supported by a Packard Fellowship for Science and Engineering.

**Author Contributions** R.I. constructed and validated the nanobody biosensors, carried out most of the cell biological experiments and analysis, contributed to overall experimental strategy and took a lead role in writing the manuscript. J.C.T. carried out early experiments identifying endocytic inhibitor effects on cellular cAMP signalling, and contributed to initial project planning. J.R.T. built the luminometer system, developed software for analysis of luminometry data, and contributed to early experiments on cellular cAMP signalling. M.C. contributed to experimental design and data analysis, and modelled effects of endocytic inhibitors on the cellular cAMP response. J.P.M. contributed to the production of receptor-containing rHDL particles and carried out *in vitro* studies of Nb80 binding and dissociation. J.S. developed the nanobody reagents used as the basis for the biosensors described in this study and advised on biosensor design and expression. S.G.F.R. contributed to developing and screening the initial nanobody reagents, and carried out *in vitro* studies of Nb80 binding and dissociation in rHDL particles reconstituted with bimane-labeled receptors. R.K.S. contributed to overall experimental interpretation, supervised J.P.M. in carrying out *in vitro* studies of Nb80 binding to receptors, and performed *in vitro* experiments evaluating Nb37 effects on G protein activation. H.E.-S. contributed to experimental design and data interpretation, and supervised efforts to model endocytic effects on the cellular cAMP response. B.H. contributed to overall experimental design and interpretation, implementation of biosensors and advised on image analysis. M.v.Z. was responsible for overall project strategy, carried out some of the imaging experiments, and drafted the manuscript together with R.I.

**Author Information** Reprints and permissions information is available at [www.nature.com/reprints](http://www.nature.com/reprints). The authors declare no competing financial interests. Readers are welcome to comment on the online version of the paper. Correspondence and requests for materials should be addressed to M.v.Z. (Mark.VonZastrow@ucsf.edu).

## METHODS

**Cell Culture, cDNA constructs and transfection.** HEK293 cells were grown in DMEM supplemented with 10% FBS (UCSF Cell Culture Facility) without antibiotics. Stably transfected HEK293 cell clones expressing Flag-tagged  $\beta_2$ -AR-3S were created using previously described Flag-tagged  $\beta_2$ -AR<sup>30</sup>. A plasmid encoding a cyclic permuted luciferase reporter construct, based on a mutated RII $\beta$  cAMP-binding domain from PKA (pGloSensor-20F, Promega). Nb80-eGFP and Nb37-eGFP were created by amplifying Nb80 and Nb37 nanobody complementary DNAs using 5'-CTTGAAAAGCTTGCCGCCACCATGGGACAGGTGCAGCTGCA-3'; 5'-TTCAAGGGATCCATGTGATGGTGTGATGGTGGTGTGAGGAGACGGT-3' and 5'-CTTGAAAAGCTTGCCGCCACCATGGGACAGGTGCAGCTGCA-3'; 5'-TTCAAGGGATCCATGTGATGGGCTTCAGGTTCTGTGATGGTGTGATG-3' primers, respectively, and cloning into the pEGFP-N1 vector using HindIII and BamHI.  $\beta$ -arrestin-2-GFP, clathrin-DsRed, EEA1-DsRed and  $G_{\alpha_s}$ -HA were gifts from M. Caron, W. Almers, K. Mostov and P. Wedegaertner, respectively.  $\beta$ -arrestin-2-mCherry was generated by subcloning  $\beta$ -arrestin-2 to pmCherry (Clontech) and  $\beta_2$ -AR-CFP was generated from the Flag-tagged  $\beta_2$ -AR construct. Transfections were performed using Lipofectamine 2000 (Invitrogen) according to the manufacturer's instructions. Flag-tagged human  $\beta_2$ -AR and  $\beta_2$ -AR-3S (Ser 355 Gly, Ser 356 Gly and Ser 364 Gly were mutated simultaneously) constructs were labelled with Alexa555- or Alexa488-conjugated M1 anti-Flag monoclonal antibody (Sigma) as described previously<sup>31</sup>.

**Live-cell confocal imaging.** Live cell imaging was carried out using Yokogawa CSU22 spinning disk confocal microscope with a  $\times 100$ , 1.4 numerical aperture, oil objective and a CO<sub>2</sub> and 37 °C temperature-controlled incubator. A 488 nm argon laser and a 568 nm argon/krypton laser (Melles Griot) were used as light sources for imaging GFP and Flag signals, respectively. Cells expressing both Flag-tagged receptor and the indicated nanobody-GFP were plated onto glass coverslips. Receptors were surface labelled by addition of M1 anti-Flag antibody (1:1,000, Sigma) conjugated to Alexa 555 (A10470, Invitrogen) to the media for 30 min, as described previously<sup>32</sup>. Indicated agonist (isoprenaline, Sigma) or antagonist (CGP-12177, Tocris) were added and cells were imaged every 3 s for 20 min in DMEM without phenol red supplemented with 30 mM HEPES, pH 7.4 (UCSF Cell Culture Facility). Time-lapse images were acquired with a Cascade II EM charge-coupled-device (CCD) camera (Photometrics) driven by Micro-Manager 1.4 (<http://www.micro-manager.org>).

**Live cell TIRF microscopy.** TIRF imaging was carried out as described previously<sup>33</sup>. Briefly, HEK293 cells co-expressing either Nb80-eGFP and  $\beta$ -arrestin-2-mCherry or clathrin light chain-DsRed, were imaged in DMEM without phenol red supplemented with 30 mM HEPES, pH 7.4 (UCSF Cell Culture Facility). Imaging was carried out using a Nikon TE-2000E inverted microscope with a  $\times 100$ , 1.49 numerical aperture TIRF objective, equipped for through-the-objective TIRF illumination, a 37 °C temperature-controlled stage (Bioscience Tools) and an objective warmer (Biopetechs). A 488 nm argon laser (Melles Griot) and a 543 nm helium-neon laser (Spectra Physics) were used as light sources. Time-lapse sequences were acquired with a C9100-12 camera (Hamamatsu Photonics) driven by iQ software (Andor). Cells were imaged every 3 s for 20 min.

**Image analysis and statistical analysis.** Images were saved as 16-bit TIFF files. Quantitative image analysis was carried out on unprocessed images using ImageJ software (<http://rsb.info.nih.gov/ij/>). Co-localization analysis was estimated by calculating the Pearson's correlation coefficient between the indicated image channels using the co-localization plug-in for ImageJ. Analysis of Nb80-GFP intensity profile along the straight line and Nb80-GFP/ $\beta$ -arrestin or Nb80-GFP/clathrin along the segmented line were carried out using the ImageJ plot profile function. For estimating changes in Nb80-GFP surface fluorescence over time in TIRF images, individual cells were selected manually and fluorescence values measured over the entire stack. A blank area of the image lacking cells was used to estimate background fluorescence. Average fluorescence intensity was measured in each frame, background-subtracted and normalized to the maximum value. *P* values are from one-tailed unpaired Student's *t*-tests. For visual presentation (but not quantitative analysis), image series were processed using Kalman stack filter in ImageJ.

**Luminescence-based rapid cAMP assay.** HEK293 cells were transfected with a plasmid encoding a cyclic-permuted luciferase reporter construct, based on a mutated RII $\beta$  cAMP-binding domain from PKA (pGloSensor-20F, Promega), which produces rapid and reversible cAMP-dependent activation of luciferase activity in intact cells. Cells were plated in 24-well dishes containing approximately 200,000 cells per well in 500  $\mu$ l DMEM without phenol red and no serum and equilibrated to 37 °C in a light-proof cabinet. An image of the plate was focused on a 512  $\times$  512 pixel electron multiplying CCD sensor (Hamamatsu C9100-13), cells were equilibrated for 1 h in the presence of 250  $\mu$ g ml<sup>-1</sup> luciferin (Biogold), and sequential luminescence images were collected every 10 s to obtain basal luminescence values. The camera shutter was closed, the cabinet opened and

the indicated concentration of isoprenaline was bath applied, with gentle manual rocking before replacing in the dark cabinet and resuming luminescence image acquisition. In endocytic manipulation experiments, cells were pre-incubated with 30  $\mu$ M Dyngo-4a (abcam Biochemicals) for 15 min. Every 10 s, sequential images were acquired using Micro-Manager (<http://www.micro-manager.org>) and integrated luminescence intensity detected from each well was calculated after background subtraction and correction for vignetting using scripts written in MATLAB (MathWorks). In each multiwell plate, and for each experimental condition, a reference value of luminescence was measured in the presence of 5  $\mu$ M forskolin, a manipulation that stimulates a moderate amount of receptor-independent activation of adenylyl cyclase. The average luminescence value—measured across duplicate wells—was normalized to the maximum luminescence value measured in the presence of 5  $\mu$ M forskolin.

**FRET imaging.** FRET imaging was carried out as described previously<sup>10</sup>. Briefly, HEK293 cells co-expressing  $\beta_2$ -AR-CFP or DRD1-CFP and Nb80-YFP were imaged in wide field at 37 °C using a shuttered mercury arc lamp and standard CFP excitation (ET430/24 $\times$ ) and YFP emission (ET500/20 $\times$ ) band pass filters (Chroma). YFP emission was collected using a 535/30 m filter, and CFP emission was collected through a 470/24 m filter. Corrected FRET ratios were obtained using the following equation:  $\text{NFRET} = [(I_{\text{FRET}} - \text{BG}_{\text{FRET}}) - (I_{\text{CFP}} - \text{BG}_{\text{CFP}}) \times \text{BT}_{\text{DONOR}} - (I_{\text{YFP}} - \text{BG}_{\text{YFP}}) \times \text{DE}_{\text{ACCEPTOR}}] / I_{\text{CFP}} \times \text{BT}_{\text{DONOR}}$ , donor bleed through;  $\text{DE}_{\text{ACCEPTOR}}$ , direct excitation of the acceptor;  $\text{BG}_X$ , background fluorescence; and  $I_X$ , integrated fluorescence intensity measured in a given channel.

**Flow cytometric assay of receptor endocytosis.** Surface fluorescence of Flag- $\beta_2$ -AR or Flag- $\beta_2$ -AR-3S expressing HEK293 cells was used to measure receptor endocytosis. Cells were incubated with 10  $\mu$ M isoprenaline for 20 min at 37 °C to drive receptor internalization to steady state and were subsequently rinsed 3 times with ice-cold PBS, then mechanically lifted and incubated with 1  $\mu$ g ml<sup>-1</sup> Alexa647 (Invitrogen)-conjugated M1 anti-Flag monoclonal antibody (Sigma) at 4 °C for 1 h. Mean fluorescence intensity of 10,000 cells was measured using a FACSCalibur instrument (Becton Dickinson). Each condition was performed in triplicate.

**Enhanced GFP calibration.** Recombinant eGFP (BioVision) was used for calibrating average fluorescence intensity of the biosensors, imaged in confocal optical sections through the cytoplasm of cells not exposed to agonist (to achieve diffuse cytoplasmic distribution of the biosensors). eGFP was diluted in Hank's balanced salt solution and confocal sections were imaged through droplets of each using the same illumination and acquisition parameters as for imaging the biosensors in cells. For each cell, a background fluorescence value was determined by average fluorescence intensity of a blank region in the same image. The cytoplasmic concentration of biosensors was estimated by interpolation of the background-subtracted value using a linear least-squares fit to the standard plot.

**Generation of  $\beta_2$ -AR-rHDL nanoparticles.** Apolipoprotein-AI (Apo-AI) was biotinylated using NHS-PEG4-biotin (Pierce Biotechnology) at a 1:1 molar ratio. Following a 30-min biotinylation reaction at room temperature, the sample was dialysed to remove free biotin. Flag-tagged  $\beta_2$ -AR was incorporated into recombinant high density lipoprotein (rHDL) particles as previously described<sup>34,35</sup> using biotinylated Apo-AI. Receptor-containing particles were then purified by M1 anti-Flag immunoaffinity chromatography<sup>36</sup>. Particles containing purified monobromobimane-labelled  $\beta_2$ -AR were generated similarly except not using biotinylated HDL, with receptor labelling and fluorescence analysis carried out as described previously<sup>18</sup>.

**Assessing Nb80 binding to immobilized  $\beta_2$ AR-rHDL.** Nb80 binding to unliganded and agonist-occupied  $\beta_2$ -AR was measured using the OctetRED biolayer interferometry system (Pall FortéBio). In this assay, a target protein is immobilized on the functionalized tip of a fibre optic probe that is dipped into an analyte solution to observe analyte association to the target protein. A dissociation step is then performed by transferring the biosensor into buffer lacking analyte. Analyte association/dissociation is measured by monitoring changes in the interference pattern of a light beam reflected from the biosensor tip as the total mass bound at the tip surface changes<sup>37</sup>. Streptavidin-coated biosensors (Pall FortéBio) were loaded with biotinylated  $\beta_2$ -AR-rHDL particles for 15 min at room temperature and the biosensors were transferred to the OctetRED instrument. Sensors were placed into assay buffer (20 mM HEPES, pH 7.7, 100 mM NaCl, 1 mM EDTA, 0.02% (w/v) ascorbic acid, 0.05% (w/v) BSA) with or without 100  $\mu$ M isoprenaline for 30 min. To measure Nb80 association, the sensor was transferred to assay buffer with Nb80 (at indicated concentrations) for 5 min, followed by a 30 min dissociation step in assay buffer. Isoprenaline (100  $\mu$ M) was included in the association and dissociation steps when measuring Nb80 binding to agonist-occupied receptor. All experiments were carried out at 25 °C with the assay plate shaking at 1,000 r.p.m. Buffer-only controls were included in each experiment to monitor for baseline drift, and nonspecific Nb80 binding was measured in a parallel assay using sensors loaded with empty rHDL particles. Raw data were

processed to remove baseline and nonspecific binding using Octet Data Analysis 7.0 software (Pall FortéBio) and exported to Prism 5 (GraphPad) for curve fitting. All association and dissociation curves were fit using a single-phase exponential association or decay curves, respectively. Equilibrium binding affinity of Nb80 for  $\beta_2$ -AR in the presence or absence of the agonist isoprenaline was assessed by monitoring the maximal interference shift generated by Nb80 binding (at varying Nb80 concentrations) to the probe containing  $\beta_2$ -AR reconstituted in rHDL. The maximal shift was plotted against the Nb80 concentration and fitted by nonlinear regression in Prism 5 (GraphPad) to generate the apparent affinity.

**Inhibition of bodipy-GTP $\gamma$ S-FL binding by Nb37.** The effect of Nb37 on GTP loading of purified G proteins was measured using 100 nM bodipy-GTP $\gamma$ S-FL (Invitrogen) essentially as described<sup>25</sup>. In this assay we used the fluorescence emission of bodipy-GTP $\gamma$ S-FL ( $\lambda_{\text{ex}} \sim 470$  nm,  $\lambda_{\text{em}} \sim 515$  nm) that accompanies binding of the labelled nucleotide to G protein<sup>38</sup>. Briefly, the fluorescence of 100 nM bodipy-GTP $\gamma$ S-FL was measured in the presence of 1 mM of the indicated G protein using a 96-well microtitre plate format on a M5 fluorescence plate reader (Molecular Devices). Nb37 was added together with bodipy-GTP $\gamma$ S-FL and the binding reaction was initiated by the addition of G protein (1 mM) in 20 mM Tris-HCl, pH 8.0, 3 mM MgCl<sub>2</sub>, 1 mM dithiothreitol in a final volume of 200  $\mu$ l. Bodipy-GTP $\gamma$ S-FL binding to heterotrimeric G protein included 0.1% dodecyl-maltoside (final). G $\alpha_s$  was purified as described<sup>39</sup>. G $\alpha_s\beta\gamma$  was purified as described<sup>13</sup>. Myristoylated G $\alpha_i$  was purified as described<sup>40</sup>. The time scans were limited to 240 s to minimize the accumulation of hydrolysis of the product of bodipy-GTP $\gamma$ S-FL, bodipy-phosphate<sup>41</sup>.

31. Gage, R. M., Matveeva, E. A., Whiteheart, S. W. & von Zastrow, M. Type I PDZ ligands are sufficient to promote rapid recycling of G protein-coupled receptors independent of binding to *N*-ethylmaleimide-sensitive factor. *J. Biol. Chem.* **280**, 3305–3313 (2005).
32. Puthenveedu, M. A. *et al.* Sequence-dependent sorting of recycling proteins by actin-stabilized endosomal microdomains. *Cell* **143**, 761–773 (2010).
33. Yudowski, G. A., Puthenveedu, M. A., Henry, A. G. & von Zastrow, M. Cargo-mediated regulation of a rapid Rab4-dependent recycling pathway. *Mol. Biol. Cell* **20**, 2774–2784 (2009).
34. Whorton, M. R. *et al.* A monomeric G protein-coupled receptor isolated in a high-density lipoprotein particle efficiently activates its G protein. *Proc. Natl Acad. Sci. USA* **104**, 7682–7687 (2007).
35. Kuszak, A. J. *et al.* Purification and functional reconstitution of monomeric  $\mu$ -opioid receptors: allosteric modulation of agonist binding by Gi<sub>2</sub>. *J. Biol. Chem.* **284**, 26732–26741 (2009).
36. Yao, X. *et al.* Coupling ligand structure to specific conformational switches in the  $\beta_2$ -adrenoceptor. *Nature Chem. Biol.* **2**, 417–422 (2006).
37. Abdiche, Y., Malashock, D., Pinkerton, A. & Pons, J. Determining kinetics and affinities of protein interactions using a parallel real-time label-free biosensor, the Octet. *Anal. Biochem.* **377**, 209–217 (2008).
38. McEwen, D. P., Gee, K. R., Kang, H. C. & Neubig, R. R. Fluorescent BODIPY-GTP analogs: real-time measurement of nucleotide binding to G proteins. *Anal. Biochem.* **291**, 109–117 (2001).
39. Sunahara, R. K., Tesmer, J. J., Gilman, A. G. & Sprang, S. R. Crystal structure of the adenylyl cyclase activator G $\alpha_s$ . *Science* **278**, 1943–1947 (1997).
40. Lee, E., Linder, M. E. & Gilman, A. G. Expression of G-protein  $\alpha$  subunits in *Escherichia coli*. *Methods Enzymol.* **237**, 146–164 (1994).
41. Jameson, E. E. *et al.* Real-time detection of basal and stimulated G protein GTPase activity using fluorescent GTP analogues. *J. Biol. Chem.* **280**, 7712–7719 (2005).